Numerical Star Formation
Proceedings IAU Symposium No. 270, 2010
J. Alves, B. G. Elmegreen, J. M. Girart & V. L. Trimble, eds.

DOI: 00.0000/X000000000000000X

Modeling High-Mass Star Formation and Ultracompact H II Regions

Ralf S. Klessen[1], Thomas Peters[1], Robi Banerjee[1], Mordecai-Mark Mac Low[2], Roberto Galván-Madrid[3,4] & Eric R. Keto[3]

[1]Zentrum für Astronomie der Universität Heidelberg, Institut für Theoretische Astrophysik, Albert-Ueberle-Str. 2, D-69120 Heidelberg, Germany

[2]Department of Astrophysics, American Museum of Natural History, 79th Street at Central Park West, New York, New York 10024-5192, USA

[3] Harvard-Smithsonian Center for Astrophysics, 60 Garden Street, Cambridge, MA 02138, USA

[4] Centro de Radioastronomía y Astrofísica, UNAM, A.P. 3-72 Xangari, Morelia 58089, Mexico

Abstract. Massive stars influence the surrounding universe far out of proportion to their numbers through ionizing radiation, supernova explosions, and heavy element production. Their formation requires the collapse of massive interstellar gas clouds with very high accretion rates. We discuss results from the first three-dimensional simulations of the gravitational collapse of a massive, rotating molecular cloud core that include heating by both non-ionizing and ionizing radiation. Local gravitational instabilities in the accretion flow lead to the build-up of a small cluster of stars. These lower-mass companions subsequently compete with the high-mass star for the same common gas reservoir and limit its overall mass growth. This process is called fragmentation-induced starvation, and explains why massive stars are usually found as members of high-order stellar systems. These simulations also show that the H II regions forming around massive stars are initially trapped by the infalling gas, but soon begin to fluctuate rapidly. Over time, the same ultracompact H II region can expand anisotropically, contract again, and take on any of the observed morphological classes. The total lifetime of H II regions is given by the global accretion timescale, rather than their short internal sound-crossing time. This solves the so-called lifetime problem of ultracompact H II region. We conclude that the the most significant differences between the formation of low-mass and high-mass stars are all explained as the result of rapid accretion within a dense, gravitationally unstable flow.

Keywords. Keyword1, keyword2, keyword3, etc.

1. Introduction

High-mass stars form in denser and more massive cloud cores (Motte et al. 2008) than their low-mass counterparts (Myers et al. 1986). High densities result in the large accretion rates, exceeding 10^{-4} $M_\odot$ yr^{-1}, required for massive stars to reach their final mass before exhausting their nuclear fuel (Keto & Wood 2006). High densities also result in local gravitational instabilities in the accretion flow, resulting in the formation of multiple additional stars (Klessen & Burkert 2000, 2001; Klessen 2001; Kratter & Matzner 2006). Young massive stars almost always have companions (Ho & Haschick 1981), and the number of their companions significantly exceeds those of low-mass stars (Zinnecker & Yorke 2007). Such companions influence subsequent accretion onto the initial star (Krumholz et al. 2009). Observations show an upper mass limit of about $100\,M_\odot$. It remains unclear whether limits on internal stability or termination of accretion by stellar feedback determines the value of the upper mass limit (Zinnecker & Yorke 2007).

H II regions form around accreting protostars once they exceed $\sim 10\,\mathrm{M}_\odot$, equivalent to a spectral type of early B. Thus, accretion and ionization must occur together in the formation of massive stars. The pressure of the 10^4 K ionized gas far exceeds that in the 10^2 K accreting molecular gas, creating unique feedback effects such as ionized outflows (Keto 2002, 2003, 2007).

Around the most luminous stars the outward radiation pressure force can equal the inward gravitational attraction. A spherically symmetric calculation of radiation pressure on dust yields equality at just under 10 $\mathrm{M}_\odot$ (Wolfire & Cassinelli 1987). However, the dust opacity is wavelength dependent, the accretion is non-spherical, the mass-luminosity ratio is different for multiple companions than for a single star, and to stop accretion more than static force balance is required. The momentum of any part of the accretion flow must be reversed (Larson & Starrfield 1971; Kahn 1974; Yorke & Krügel 1977; Nakano et al. 1995). Observations by Keto & Wood (2006) provide evidence for the presence of all these mitigating factors, and numerical experiments combining some of these effects (Yorke & Sonnhalter 2002; Krumholz et al. 2007) confirm their effectiveness, showing that radiation pressure is not dynamically significant below the Eddington limit.

The most significant differences between massive star formation and low-mass star formation seem to be the clustered nature of star formation in dense accretion flows and the ionization of these flows. We present results from three-dimensional simulations by Peters et al. (2010a,b,c) of the collapse of molecular cloud cores to form a cluster of massive stars that include ionization feedback. These calculations are the first ones that allow us to study these effects simultaneously.

2. Modeling High-Mass Star Formation

Our discussion is based on a series of recent numerical simulations by Peters et al. (2010a,b,c). They are based on a modified version of the adaptive-mesh code FLASH (Fryxell et al. 2000) that has been extended to include sink particles representing protostars (Federrath et al. 2010). The protostars evolve following a prestellar model that determines their stellar and accretion luminosities as function of protostellar mass and accretion rate. We set the stellar luminosity with the zero-age main sequence model by Paxton (2004) and the accretion luminosity by using the tables by Hosokawa & Omukai (2009). The ionizing and non-ionizing radiation from the protostars is propagated through the gas using an improved version of the hybrid characteristics raytracing method on the adaptive mesh developed by Rijkhorst et al. (2006). In some calculations, secondary sink formation is suppressed with a density-dependent temperature floor to prevent runaway collapse of dense blobs of gas. For further details, consult Peters et al. (2010a).

The simulations start with a $1000\,M_\odot$ molecular cloud. The cloud has a constant density core of $\rho = 1.27 \times 10^{-20}\ \mathrm{g\,cm^{-3}}$ within a radius of $r = 0.5\,\mathrm{pc}$ and then falls off as $r^{-3/2}$ until $r = 1.6\,\mathrm{pc}$. The initial temperature of the cloud is $T = 30\,\mathrm{K}$. The whole cloud is set up in solid body rotation with an angular velocity $\omega = 1.5 \times 10^{-14}\,\mathrm{s^{-1}}$ corresponding to a ratio of rotational to gravitational energy $\beta = 0.05$ and a mean specific angular momentum of $j = 1.27 \times 10^{23}\,\mathrm{cm^2 s^{-1}}$. Peters et al. (2010a,b,c) follow the gravitational collapse of the molecular cloud with the adaptive mesh until they reach a cell size of 98 AU. Then sink particles are created at a cut-off density of $\rho_{\mathrm{crit}} = 7 \times 10^{-16}\,\mathrm{g\,cm^{-3}}$. All gas within the accretion radius of $r_{\mathrm{sink}} = 590\,\mathrm{AU}$ above ρ_{crit} is accreted to the sink particle if it is gravitationally bound to it. The Jeans mass on the highest refinement level is $M_{\mathrm{jeans}} = 0.13\,\mathrm{M}_\odot$. A summary of the three simulations discussed in this proceedings article is provided in Table 1.

Table 1. Overview of collapse simulations.

Name	Resolution	Radiative Feedback	Multiple Sinks	$M_{\rm sinks}\,(M_\odot)$	$N_{\rm sinks}$	$M_{\rm max}\,(M_\odot)$
Run A	98 AU	yes	no	72.13	1	72.13
Run B	98 AU	yes	yes	125.56	25	23.39
Run D	98 AU	no	yes	151.43	37	14.64

3. Fragmentation-Induced Starvation

In this section we compare the protostellar mass growth rates from three different calculations. Run A only allows for the formation of a single sink particle, Run B has multiple sinks and radiative heating, while Run D has multiple sinks but no radiative heating. As already discussed by Peters et al. (2010a), when only the central sink particle is allowed to form (Run A), nothing stops the accretion flow to the center. Figure 1 shows that the central protostar grows at a rate $\dot{M} \approx 5.9 \times 10^{-4}\,M_\odot\,{\rm yr}^{-1}$ until we stop the calculation when the star has reached $72\,M_\odot$. The growing star ionizes the surrounding gas, raising it to high pressure. However this hot bubble soon breaks out above and below the disk plane, without affecting the gas flow in the disk midplane much. In particular, it cannot halt the accretion onto the central star. Similar findings have also been reported from simulations focussing on the effects of non-ionizing radiation acting on smaller scales (Yorke & Sonnhalter 2002; Krumholz et al. 2007, 2009; Sigalotti et al. 2009). Radiation pressure cannot stop accretion onto massive stars and is dynamically unimportant, except maybe in the centers of dense star clusters near the Galactic center.

The situation is different when the disk can fragment and form multiple sink particles. Initially the mass growth of the central protostar in Runs B and D is comparable to the one in Run A. However, as soon as further protostars form in the gravitationally unstable disk, they begin to compete with the central object for accretion of disk material. Unlike in the classical competitive accretion picture (Bonnell et al. 2001a, 2004), it is not the most massive object that dominates and grows disproportionately fast. On the contrary, it is the successive formation of a number of low-mass objects in the disk at increasing radii that limits subsequent growth of the more massive objects in the inner disk. Material that moves inwards through the disk due to viscous and gravitational torques accretes preferentially onto the sinks at larger radii.

Similar behavior is found in models of low-mass protobinary disks, where again the secondary accretes at a higher rate than the primary. Its orbit around the common center of gravity scans larger radii and hence it encounters material that moves inwards through the disk before the primary star. This drives the system towards equal masses and circular orbits (Bate 2000). In our simulations, after a certain transition period hardly any gas makes it all the way to the center and the accretion rate of the first sink particle drops to almost zero. This is the essence of the fragmentation-induced starvation process. In Run B, it prevents any star from reaching a mass larger than $25\,M_\odot$. The Jeans mass in Run D is smaller than in Run B because of the lack of accretion heating, and consequently the highest mass star in Run D grows to less than $15\,M_\odot$.

Inspection of Figure 1 reveals additional aspects of the process. We see that the total mass of the sink particle system increases at a faster rate in the multiple sink simulations, Runs B and D, than in the single sink case, Run A. This is understandable, because as more and more gas falls onto the disk it becomes more and more unstable to fragmentation, so as time goes by additional sink particles form at larger and larger radii. Star formation occurs in a larger volume of the disk, and mass growth is not limited by the

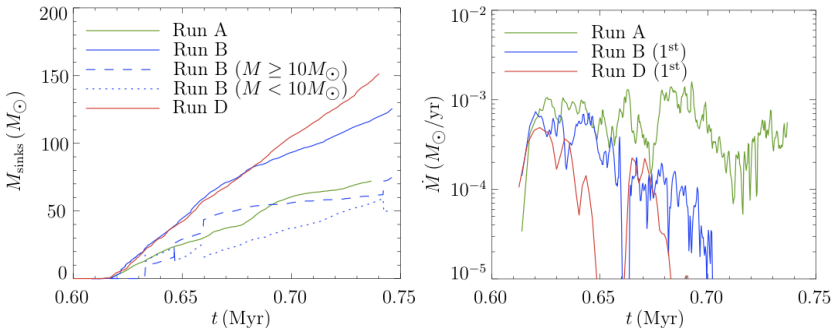

Figure 1. *left* Total accretion history of all sink particles combined forming in Runs A, B, and D. *right* Instantaneous accretion rate as function of time of the first sink particle to form in the three runs.

disk's ability to transport matter to its center by gravitational or viscous torques. As a result the overall star-formation rate is larger than in Run A.

Since the accretion heating raises the Jeans mass and length in Run B, the total number of sink particles is higher in Run D than in B, and the stars in Run D generally reach a lower mass than in Run B. These two effects cancel out to lead to the same overall star formation rate for some time. Eventually, however, the total accretion rate of Run B drops below that of Run D. At time $t \approx 0.68\,$Myr the accretion flow around the most massive star has attenuated below the value required to trap the H II region. It is able to break out and affect a significant fraction of the disk area. A comparison with the mass growth of Run D clearly shows that there is still enough gas available to continue constant cluster growth for another 50 kyr or longer, but the gas can no longer collapse in Run B. Instead, it is swept up in a shell surrounding the expanding H II region. The figure furthermore demonstrates that, although the accretion rates of the most massive stars ($M \geqslant 10\,{\rm M}_\odot$) steadily decrease, the low-mass stars ($M < 10\,{\rm M}_\odot$), which do not produce any significant H II regions, keep accreting at the same rate.

4. Properties of the H II Regions

In all calculations by Peters et al. (2010a,c), the H II regions are gravitationally trapped in the disk plane but drive a bipolar outflow perpendicular to the disk. The highly variable rate of accretion onto protostars as they pass through dense filaments causes fast ionization and recombination of large parts of the interior of the perpendicular outflow. The H II regions around the massive protostars do not uniformly expand, but instead rapidly fluctuate in size, shape and luminosity.

We can directly compare these numerical models with radio observations of free-free continuum, hydrogen recombination lines, and $NH_3(3,3)$ rotational lines by generating synthetic maps (Peters et al. 2010a,b). The simulated observations of radio continuum emission reproduce the morphologies reported in surveys of ultracompact H II regions (Wood & Churchwell 1989; Kurtz et al. 1994). Figure 2 shows typical images from Run B to illustrate this point. It is important to note that even the correct relative numbers of the different morphological types are obtained. Table 2 shows the morphology statistics of UC H II regions in the surveys of Wood & Churchwell (1989) and Kurtz et al. (1994) as well as from a random evolutionary sample from Runs A and B of 500 images for each simulation. While the statistics of the cluster simulation B agrees with the observational data, this is not the case for Run A, in which only one massive star forms. For further discussion, see Peters et al. (2010b).

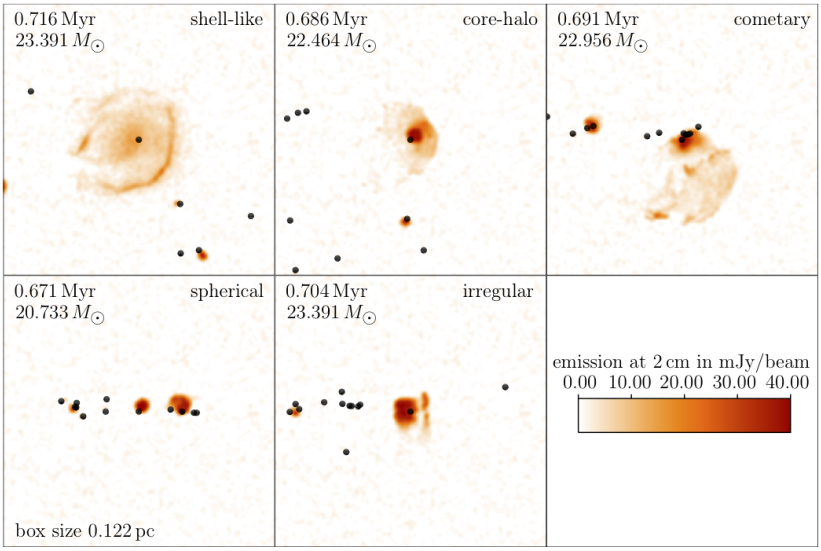

Figure 2. H II region morphologies. This figure shows ultracompact H II regions around massive protostars in Run B at different time steps and from different viewpoints. The cluster is assumed to be 2.65 kpc away, the full width at half maximum of the beam is $0\farcs14$ and the noise level is 10^{-3} Jy. This corresponds to typical VLA parameters at a wavelength of 2 cm. The protostellar mass of the central star which powers the H II region is given in the images. The H II region morphology is highly variable in time and shape, taking the form of any observed type (Wood & Churchwell 1989; Kurtz et al. 1994) during the cluster evolution.

Table 2. Percentage Frequency Distribution of Morphologies

Type	Wood & Churchwell (1989)	Kurtz et al. (1994)	Run A	Run B
Spherical/Unresolved	43	55	19	60 ± 5
Cometary	20	16	7	10 ± 5
Core-halo	16	9	15	4 ± 2
Shell-like	4	1	3	5 ± 1
Irregular	17	19	57	21 ± 5

The H II regions in the model fluctuate rapidly between different shapes while accretion onto the protostar continues. When the gas reservoir around the two most massive stars is exhausted, their H II regions merge into a compact H II region, the type that generally accompanies observed ultracompact H II regions (Kim & Koo 2001). These results suggest that the lifetime problem of ultracompact H II regions (Wood & Churchwell 1989) is only apparent. Since H II regions embedded in accretion flows are continuously fed, and since they flicker with variations in the flow rate, their size does not depend on their age until late in their lifetimes.

To compare more directly to observations of the time variability of H II regions, Peters et al. (2010b) analyze a few time intervals of interest at a resolution of 10 years. They find that when the accretion rate to the star powering the H II region has a large, sudden increase, the ionized region shrinks, and then slowly re-expands. This agrees with the contraction, changes in shape, or anisotropic expansion observed in radio continuum observations of ultracompact H II regions over intervals of ~ 10 yr (Franco-Hernández & Rodríguez 2004; Rodríguez et al. 2007; Galván-Madrid et al. 2008). Figure 3 shows the 2-cm continuum flux, the characteristic size of the H II region, and the rate of accretion

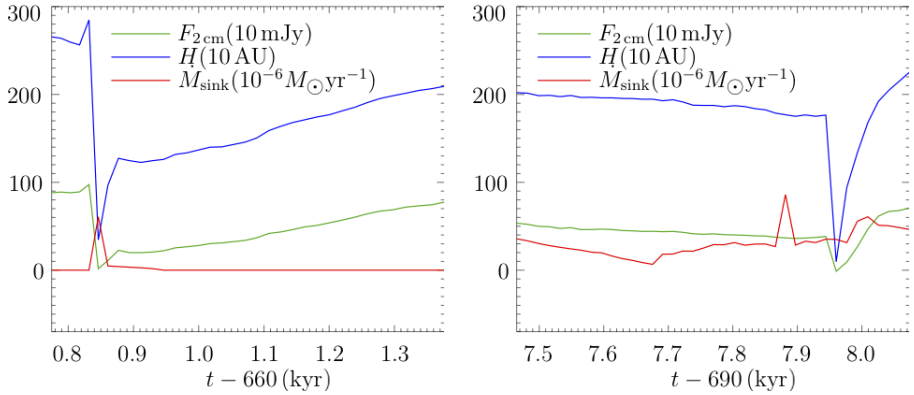

Figure 3. Time variability of the accretion flow and H II region. The image shows accretion rate onto the sink particle $\dot{M}_{\mathrm{sink}}$ (sink particle, in units of $10^{-6}\,\mathrm{M}_\odot\,\mathrm{yr}^{-1}$), corresponding diameter H of the H II region (in units of 10 AU), as well as the resulting 2-cm continuum flux $F_{2\mathrm{cm}}$ (in units of 10 mJy) for two selected time periods in Run B.

onto the star. In the left panel, the H II region is initially relatively large, and accretion is almost shut off. A sudden strong accretion event causes the H II region to shrink and decrease in flux. The star at this moment has a mass of $19.8\,\mathrm{M}_\odot$. In the right panel, the star has a larger mass ($23.3\,\mathrm{M}_\odot$), the H II region is initially smaller, and the star is constantly accreting gas. The ionizing-photon flux appears to be able to ionize the infalling gas stably, until a peak in the accretion rate by a factor of 3 and the subsequent continuos accretion of gas makes the H II region to shrink and decrease in flux. The H II region does not shrink immediately after the accretion peak because the increase is relatively mild and the geometry of the infalling gas permitted ionizing photons to escape in one direction. These results show that observations of large, fast changes in ultracompact H II regions (Franco-Hernández & Rodríguez 2004; Rodríguez et al. 2007; Galván-Madrid et al. 2008) are controlled by the accretion process.

5. Comparison with W51e2

The Peters et al. (2010a) model can be compared with the well-studied ultracompact H II region W51e2 (Zhang et al. 1998; Keto & Klaassen 2008). In Figure 4 we show simulated and observed maps of the $NH_3(3,3)$ emission, the 1.3 cm thermal continuum emission, and the H53α radio recombination line. The simulated maps were made at a time when the first star in Run B has reached a mass of $20\,\mathrm{M}_\odot$.

The brightest $NH_3(3,3)$ emission reveals the dense accretion disk surrounding the most massive star in the model, one of several within the larger-scale rotationally flattened flow. The disk shows the signature of rotation, a gradient from redshifted to blueshifted velocities across the star. A rotating accretion flow is identifiable in the observations, oriented from the SE (red velocities) to the NW (blue velocities) at a projection angle of 135° east of north (counterclockwise).

The 1.3 cm radio continuum traces the ionized gas, which in the model expands perpendicularly to the accretion disk down the steepest density gradient. As a result, the simulated map shows the brightest radio continuum emission just off the mid-plane of the accretion disk, offset from the central star rather than surrounding it spherically. Continuum emission in the observations is indeed offset from the accretion disk traced in ammonia. The $NH_3(3,3)$ in front of the H II region is seen in absorption and red-shifted

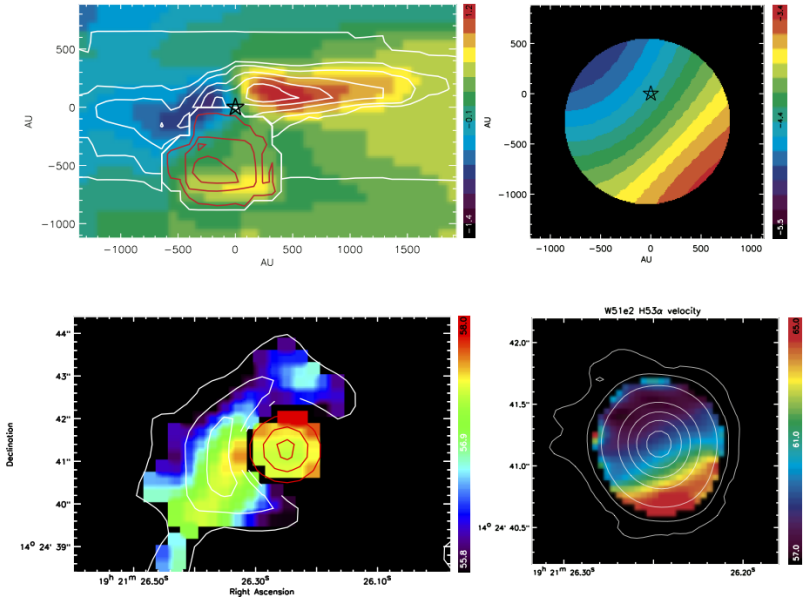

Figure 4. Comparison of line and continuum emission simulated from the model (upper panels) and actually observed from the W51e2 region (lower panels). The left panels show the $NH_3(3,3)$ line emission strength in white contours, the molecular line velocities as the background color, and the 1.3 cm free-free continuum from ionized gas in red contours. The right panels show the H53α recombination line velocities from the ionized gas. The molecular line observations are from Zhang et al. (1998) and the H53α observations from Keto & Klaassen (2008). For further details see Peters et al. (2010a).

by its inward flow toward the protostar. The density gradient in the ionized flow determines the apparent size of the H II region. Therefore the accretion time scale determines the age of the H II region rather than the much shorter sound-crossing time.

Photoevaporation of the actively accreting disk supplies the ionized flow. Therefore, the ionized gas rotates as it flows outward, tracing a spiral. An observation that only partially resolves the spatial structure of the ionized flow sees a velocity gradient oriented in a direction between that of rotation and of outflow, as shown in the simulated observation. The observed H53α recombination line (Keto & Klaassen 2008) in Figure 4 indeed shows a velocity gradient oriented between the directions of rotation and the outflow.

6. Conclusions

Numerical simulations of high-mass star formation regions are now able to resolve the collapse of massive molecular cloud cores and the accretion flow onto the central group of protostars while at the same time treating the transport of ionizing and non-ionizing radiation. This allows us to consistently follow the dynamical evolution of the H II regions that ubiquitously accompany the birth of massive stars. We find that the accretion flow becomes gravitationally unstable and fragments. Secondary star formation sets in and consumes material that would otherwise be accreted by the massive star in the center. We call this process fragmentation-induced starvation. It determines the upper mass limit of the stars in the system and explains why massive stars are usually found as members of larger clusters. These simulations furthermore show that the H II regions forming around massive stars are initially trapped by the infalling gas. But soon, they begin to fluctuate. Over time, the same ultracompact H II region can expand anisotropically,

contract again, and take on any of the observed morphological classes. The total lifetime of H II regions thus is given by the global accretion timescale, rather than their short internal sound-crossing time. This solves the so-called lifetime problem of ultracompact H II regions.

References

Bate, M. R. 2000, Mon. Not. R. Astron. Soc., 314, 33
Bonnell, I. A., Bate, M. R., Clarke, C. J., & Pringle, J. E. 2001a, Mon. Not. R. Astron. Soc., 323, 785
Bonnell, I. A., Vine, S. G., & Bate, M. R. 2004, Mon. Not. R. Astron. Soc., 349, 735
Federrath, C., Banerjee, R., Clark, P. C., & Klessen, R. S. 2010, Astrophys. J., 713, 269
Franco-Hernández, R. & Rodríguez, L. F. 2004, Astrophys. J., 604, L105
Fryxell, B., Olson, K., Ricker, P., et al. 2000, Astrophys. J. Suppl. Ser., 131, 273
Galván-Madrid, R., Rodríguez, L. F., Ho, P. T. P., & Keto, E. 2008, Astrophys. J., 674, L33
Ho, P. T. P. & Haschick, A. D. 1981, Astrophys. J., 248, 622
Hosokawa, T. & Omukai, K. 2009, Astrophys. J., 691, 823
Kahn, F. D. 1974, Astron. Astrophys., 37, 149
Keto, E. 2002, Astrophys. J., 580, 980
Keto, E. 2003, Astrophys. J., 599, 1196
Keto, E. 2007, Astrophys. J., 666, 976
Keto, E. & Klaassen, P. 2008, Astrophys. J., 678, L109
Keto, E. & Wood, K. 2006, Astrophys. J., 637, 850
Kim, K.-T. & Koo, B.-C. 2001, Astrophys. J., 549, 979
Klessen, R. S. 2001, Astrophys. J., 556, 837
Klessen, R. S. & Burkert, A. 2000, Astrophys. J. Suppl. Ser., 128, 287
Klessen, R. S. & Burkert, A. 2001, Astrophys. J., 549, 386
Kratter, K. M. & Matzner, C. D. 2006, Mon. Not. R. Astron. Soc., 373, 1563
Krumholz, M. R., Klein, R. I., & McKee, C. F. 2007, Astrophys. J., 656, 959
Krumholz, M. R., Klein, R. I., McKee, C. F., Offner, S. S. R., & Cunningham, A. J. 2009, Science, 323, 754
Kurtz, S., Churchwell, E., & Wood, D. O. S. 1994, Astrophys. J. Suppl. Ser., 91, 659
Larson, R. B. & Starrfield, S. 1971, Astron. Astrophys., 13, 190
Motte, F., Bontemps, S., Schneider, N., Schilke, P., & Menten, K. M. 2008, in Astronomical Society of the Pacific Conference Series, Vol. 387, Massive Star Formation: Observations Confront Theory, ed. H. Beuther, H. Linz, & T. Henning, 22–29
Myers, P. C., Dame, T. M., Thaddeus, P., et al. 1986, Astrophys. J., 301, 398
Nakano, T., Hasegawa, T., & Norman, C. 1995, Astrophys. J., 450, 183
Paxton, B. 2004, Publ. Astron. Soc. Pac., 116, 699
Peters, T., Banerjee, R., Klessen, R. S., Mac Low, M.-M., Galván-Madrid, R., & Keto, E. R. 2010a, Astrophys. J., 711, 1017
Peters, T., Mac Low, M.-M., Banerjee, R., Klessen, R. S., & Dullemond, C. P. 2010b, Astrophys. J., in press
Peters, T., Klessen, R. S., Banerjee, R., & Mac Low, M.-M. 2010c, Astrophys. J., submitted
Rijkhorst, E.-J., Plewa, T., Dubey, A., & Mellema, G. 2006, Astron. Astrophys., 452, 907
Rodríguez, L. F., Gómez, Y., & Tafoya, D. 2007, Astrophys. J., 663, 1083
Sigalotti, L. D. G., de Felice, F., & Daza-Montero, J. 2009, Astrophys. J., 707, 1438
Wolfire, M. G. & Cassinelli, J. P. 1987, Astrophys. J., 319, 850
Wood, D. O. S. & Churchwell, E. 1989, Astrophys. J. Suppl. Ser., 69, 831
Yorke, H. W. & Krügel, E. 1977, Astron. Astrophys., 54, 183
Yorke, H. W. & Sonnhalter, C. 2002, Astrophys. J., 569, 846
Zhang, Q., Ho, P. T. P., & Ohashi, N. 1998, Astrophys. J., 494, 636
Zinnecker, H. & Yorke, H. W. 2007, Ann. Rev. Astron. Astrophys., 45, 481